Available online at www.sciencedirect.com
ScienceDirect
Journal of Power Sources 166 (2007) 492–498
JOURNAL OF POWER SOURCES
www.elsevier.com/locate/jpowsour

Enhanced high rate performance of $LiMn_2O_4$ spinel nanoparticles synthesized by a hard-template route

J. Cabana [a], T. Valdés-Solís [b], M.R. Palacín [a], J. Oró-Solé [a], A. Fuertes [a], G. Marbán [b], A.B. Fuertes [b,*]

[a] *Institut de Ciència de Materials de Barcelona (CSIC), Campus UAB, E-08193 Bellaterra, Catalonia, Spain*
[b] *Instituto Nacional del Carbón (CSIC), Francisco Pintado Fe 26, 33011 Oviedo, Spain*

Received 17 July 2006; received in revised form 15 December 2006; accepted 28 December 2006
Available online 2 February 2007

Abstract

A nanosized $LiMn_2O_4$ (nano-$LiMn_2O_4$) spinel was prepared by a novel route using a porous silica gel as a sacrificial hard template. This material was found to be made up of 8–20 nm nanoparticles with a mean crystallite size of 15 nm. The electrochemical properties of nano-$LiMn_2O_4$ were tested in lithium cells at different cycling rates and compared to those of microsized $LiMn_2O_4$ (micro-$LiMn_2O_4$) obtained by the classical solid state route. Microsized $LiMn_2O_4$ is formed by 3–20 μm agglomerates, the size of each individual particle being approximately 0.20 μm. The behaviour of nano-$LiMn_2O_4$ as a positive electrode improves with increasing current densities (from *C*/20 to 2*C*). Moreover, it was found to exhibit a noticeably better performance at high rates (2*C*), with higher initial capacity values and very good retention (only 2% loss after 30 cycles), with respect to micro-$LiMn_2O_4$, almost certainly due to enhanced lithium diffusion in the small particles.

Keywords: Lithium batteries; $LiMn_2O_4$; Lithium manganese spinel; Template method; Silica gel

1. Introduction

Lithium-ion batteries are now well established in the market as the preferred rechargeable power source for portable electronics. This technology is currently also one of the most promising for use in electrical or hybrid vehicles, or for storing the energy obtained from renewable sources, provided that the power and energy densities it delivers can be improved. Even though commercial batteries still consist mainly of the $LiCoO_2$/C system originally developed in 1990 by Sony Corp. [1], a huge amount of work has been devoted to finding alternative electrode materials in order to improve performance, safety, cost or environmental compatibility [2]. These studies have opened up a very wide spectrum of alternative electrode and electrolyte materials, leading in some cases to the discovery of new reaction pathways with lithium [3] that deviate from the classical insertion or alloying mechanisms. One of the first alternative positive electrode materials investigated was $LiMn_2O_4$, which had already been studied by Thackeray et al. in the 1980s [4,5]. This compound has significant advantages over $LiCoO_2$ in terms of toxicity and cost. Moreover, the natural abundance of manganese and the familiarity of battery manufacturers with the chemistry of manganese oxides, used in primary alkaline cells, made the choice of $LiMn_2O_4$ even more attractive. The interest aroused in the scientific community is reflected in the more than 1500 research papers published on this compound from 1990 to the present time, compared to only four before 1990. However, its practical application was found to be much more difficult than expected due to the complex chemistry of spinels [6,7], associated with problems of nonstoichiometry and electrochemical stability under diverse real application conditions. Nevertheless, even though the road to the optimization of this material has been long and winding [8], and other interesting materials such as layered $LiM_xM'_yM''_zO_2$ phases (M, M′, M″ = Mn, Ni, Co; $x+y+z=1$) or low cost olivine $LiFePO_4$ are certainly competitive [9], $LiMn_2O_4$ still remains a valid choice for the fabrication of reliable lithium-ion batteries. Indeed, recent results [10] indicate that the performance of this compound is greatly improved when LiBOB electrolyte salt instead of $LiPF_6$ is used

* Corresponding author. Tel.: +34 985 119 090; fax: +34 985 297 662.
E-mail address: abefu@incar.csic.es (A.B. Fuertes).

0378-7753/$ – see front matter © 2007 Elsevier B.V. All rights reserved.
doi:10.1016/j.jpowsour.2006.12.107

to avoid the formation of traces of HF that lead to Mn^{3+} leaching [11]. Moreover, very promising results are reported [12] for a 2.5 V $LiMn_2O_4$/PVDF-based electrolyte gel/$Li_4Ti_5O_{12}$ cell which exhibits appreciable capacity values at diverse rates together with a high stability and a remarkable cycle life.

In recent years, a widely used approach to enhance the performance of electrode materials has been to reduce the particle size to nanoscale [13]. The aim is to favour diffusion of lithium through the particles (i.e., enhanced conductivity and rate capabilities), and to allow a more effective use of the material (i.e., higher specific capacities). This has led, in some cases, to the discovery of a new and exciting reactivity of the materials studied [14]. The case of $LiMn_2O_4$ is clearly not an exception to this current trend. A wide variety of synthetic routes have been chosen, to date, in order to obtain $LiMn_2O_4$ in the form of nanoparticles, e.g. combustion [15,16], ultrasonic spray pyrolysis [17], ball-milling [18], sol–gel [19] or solution methods [20–22]. In general, taking into account only the first cycle when different particle sizes are compared, expectations appear to have been fulfilled in terms of specific capacity [15,18,20] and rate capabilities [16,18,23,24] (i.e., the nanometric samples show higher initial capacity values at higher regimes than the micrometric ones). Nevertheless, it is not clear whether reducing the particle size is beneficial [19] or detrimental [17,18,20,25] for the capacity retention upon long-term cycling at high voltages and at a given rate, as undesired side reactivity with the electrolyte due to a high specific surface has already been mentioned as a major drawback for the use of as-prepared materials at the nanometric scale [13]. However, to the best of our knowledge, very little attention has been paid to the effect of different charge–discharge rates on the capacity retention of samples of $LiMn_2O_4$ of a very different particle size (nanometric versus micrometric) when cycled in the 4 V region. The above mentioned enhanced kinetics of lithium exchange should allow the use of higher current densities to be used without any significant loss (contrary to what occurs in micrometric samples).

Recently, hard-template synthesis has been revealed as a straightforward procedure for the preparation of high-surface area inorganic compounds (nanoparticles or nanostructures) [26–28]. Usually, this synthetic strategy comprises three steps: (i) infiltration of the porosity of the template with a solution containing the precursors of the inorganic compound; (ii) heat treatment of the impregnated template under a controlled atmosphere to convert the infiltrated precursor into the inorganic material; (iii) removal of the template framework. The key feature of this synthetic method is that the formation of inorganic materials, which normally requires heat treatments at high temperatures, takes place in the confined nanospaces provided by the pores of a solid (hard template). Under these circumstances, the sintering of the formed solid is restricted and high-surface area materials are achieved. Two types of solids have been currently employed as hard-templates, i.e. porous silica and porous carbon [27–30]. In particular, the use of mesoporous silica gel as template is of great interest due to its ready availability, low-cost and inertness. Recently, silica xerogel was employed as template for the preparation of simple [29] and mixed oxides (spinels and perovskites) [31].

In the present work we propose the use of a porous silica gel as template for preparing $LiMn_2O_4$ spinel nanoparticles, in a novel and simple approach for the synthesis of this material. Our aim was to test its properties as a positive electrode material in a lithium battery, focusing on possible improvements with the respect to a sample prepared by a conventional solid state route, especially when high rates are used.

2. Experimental

2.1. Preparation of materials

2.1.1. Preparation of $LiMn_2O_4$ nanoparticles (nano-$LiMn_2O_4$)

A commercial silica gel (Aldrich 28,851-9) was employed as hard template for the synthesis of nano-$LiMn_2O_4$. This silica has a BET surface area of 340 $m^2\,g^{-1}$ and a pore volume of 0.89 $cm^3\,g^{-1}$. The porosity of this material is made up of mesopores with a size of around 12 nm as deduced by the pore size distribution obtained from the analysis of the adsorption branch of the nitrogen sorption isotherm. The procedure used for the synthesis of nano-$LiMn_2O_4$ is similar to that previously reported for the preparation of inorganic materials using a silica xerogel as template [29]. For a typical synthesis, metal nitrates ($LiNO_3$ and $Mn(NO_3)_2{\cdot}6H_2O$ from Aldrich) were dissolved in ethanol (around 1.75 g nitrate (g ethanol)$^{-1}$ with a Mn/Li molar ratio of 2. Afterwards, the silica gel was impregnated with this solution until incipient wetness was attained. The impregnated sample was dried at 100 °C. The impregnation-drying cycle was repeated up to four times for a high loading of metal nitrate into the silica porosity. The impregnated samples were then calcined in air at 600 °C (5 °C min^{-1}) for 4 h. The metal oxide products were obtained after dissolution of the silica framework in a 2 M NaOH solution (24 h).

2.1.2. Preparation of $LiMn_2O_4$ microparticles (micro-$LiMn_2O_4$)

For purposes of comparison, $LiMn_2O_4$ was also prepared by a classical solid state method as reported elsewhere [32]. A stoichiometric mixture of Li_2CO_3 and electrochemically prepared manganese dioxide (EMD) was heated in air for 72 h with two intermediate grindings and a final slow cooling (20 °C h^{-1}).

2.2. Characterization of the materials

X-ray diffraction (XRD) patterns for the spinels were obtained on a Siemens D5000 instrument operating at 40 kV and 20 mA and using monochromatic Cu Kα radiation (Cu $K\alpha_1$, $\lambda = 0.15406$ nm). The crystallite size was determined by means of the Scherrer equation. Nitrogen adsorption isotherms were performed at −196 °C on a Micromeritics ASAP 2010 volumetric adsorption system. The BET surface area was deduced from the isotherm analysis in the relative pressure range of 0.04–0.20.

Electron microscopy images and electron diffraction patterns were obtained in a JEOL 1210 transmission electron microscope operating at 120 kV. The specimens for electron microscopy were prepared dispersing the powders in *n*-hexane

and depositing a droplet of this suspension on a carbon coated film supported on a copper grid. The particle sizes were estimated by observation of low resolution transmission electron images with a minimum of 50 crystals per sample. Scanning electron microscopy (SEM) was performed in a Zeiss DSM 942.

Electrochemical lithium intercalation/deintercalation tests were performed in two-electrode Swagelok® cells using lithium foil (Aldrich 99.9%) as the counter electrode. The working electrode consisted of a powder mixture of the prepared samples and 15% SuperP carbon black (kindly supplied by MMM, Belgium). Two sheets of Whatman GF/D borosilicate glass fibre soaked in 1 M LiPF6 in EC:DMC 1:1 (Merck) were used as a separator. The cells were tested using an Arbin potentiostat (Arbin Instr., USA) in galvanostatic mode at different *C*/*n* rates (equivalent to $1/n$ lithium h^{-1}), where $n = 0.5, 2, 20$.

3. Results and discussion

3.1. Structural characteristics of the materials

The product obtained by the template technique was identified by X-ray diffraction analysis ($10 \leq 2\theta \leq 90^\circ$). The XRD patterns for the synthesized materials contain the characteristic peaks for a $LiMn_2O_4$ spinel (Fig. 1a). The broad diffraction peaks of the nano-$LiMn_2O_4$ sample indicate that it is made up of very small particles. The crystallite size estimated from the broadening of the (1 1 1) peak is around 15 nm. The presence of the $LiMn_2O_4$ spinel type structure is also confirmed by Raman spectroscopy (not shown), as there are six typical characteristic absorption peaks [33,34] at around 649, 567, 467, 363, 308 and 280 cm^{-1}.

The TEM image shown in Fig. 2a clearly reveals that the $LiMn_2O_4$ spinel prepared by the template route is made up of nanoparticles with a size between 8 and 20 nm, which is in agreement with the value deduced from the XRD analysis and indicates that the particles are single crystals. The selected area electron diffraction (SAED) pattern corresponding to a group of particles is shown in Fig. 2a (inset), in which diffraction rings exhibiting *d*-values typical of the cubic $LiMn_2O_4$ spinel structure are indicated.

The SEM images obtained for the micro-$LiMn_2O_4$ spinel shows that this sample is formed by particle agglomerates that are heterogeneous in size (3–20 μm, see Fig. 2c). TEM inspection indicates that the individual particles have sizes between 60 and 500 nm (Fig. 2b), the mean values being around 0.20 μm. The SAED patterns confirm the cubic structure of $LiMn_2O_4$ with the $Fm\bar{3}m$ space group and a cell parameter close to 8.2 Å (see the pattern corresponding to the (1 0 0) zone axis in Fig. 2b, inset).

Fig. 1b shows the nitrogen sorption isotherm obtained for the nano-$LiMn_2O_4$ sample. The BET surface area obtained is of 88 $m^2\,g^{-1}$, a value which, as expected, is considerably larger than that obtained for the micro-$LiMn_2O_4$ sample (1.3 $m^2\,g^{-1}$). The isotherm plotted in Fig. 1b does not exhibit any capillary condensation steps but it does exhibit a large nitrogen uptake at high relative pressures ($p/p_0 > 0.8$). These findings suggest that the nano-$LiMn_2O_4$ sample does not contain framework-confined pores but is rather made up of individual nanoparticles. This is in agreement with the conclusions reached from the TEM analysis (Fig. 2a). If it is assumed that the BET surface area corresponds to the external surface area, the mean size deduced for the nanoparticles is 15 nm. This value is in agreement with that estimated from the broadening of XRD peaks, and is again consistent with the particles being single crystals.

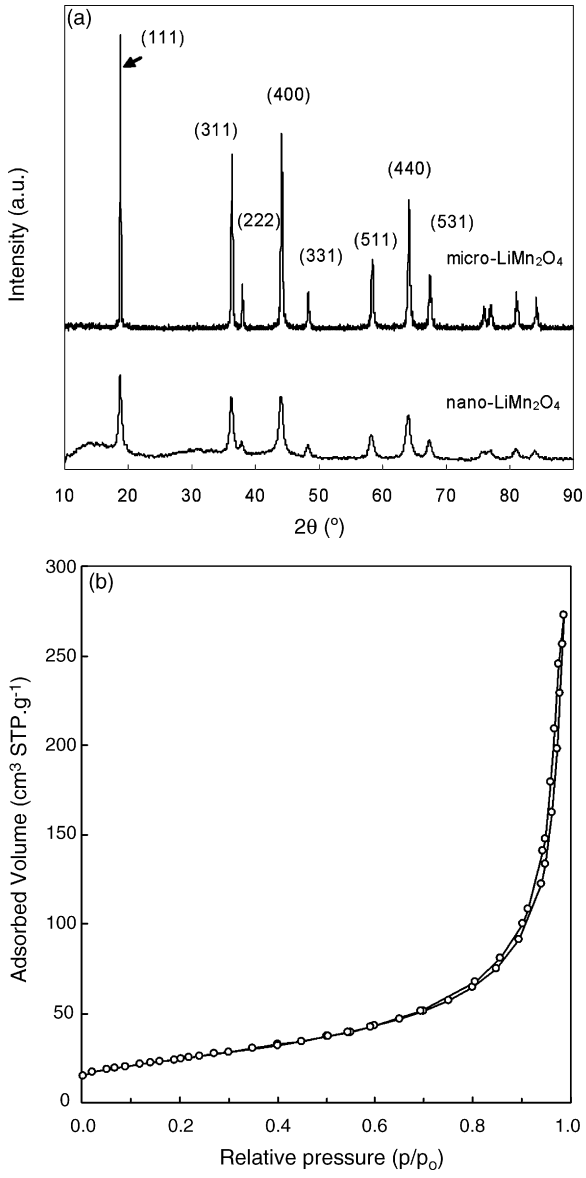

Fig. 1. (a) XRD spectra of nanometric and micrometric $LiMn_2O_4$; (b) nitrogen sorption isotherm of the nano-$LiMn_2O_4$ sample.

3.2. Electrochemical performance

Fig. 3a and b shows the first charge–discharge cycle at *C*/20 and *C*/2 regimes of $LiMn_2O_4$ samples synthesized by the template method. A higher specific capacity upon charge (137 mAh g^{-1} versus 115 mAh g^{-1}) is observed in the former, only 85% of which is recovered in the subsequent discharge. In contrast, 100% efficiency is observed for *C*/2. The different extent of irreversible side reactions with the electrolyte at high

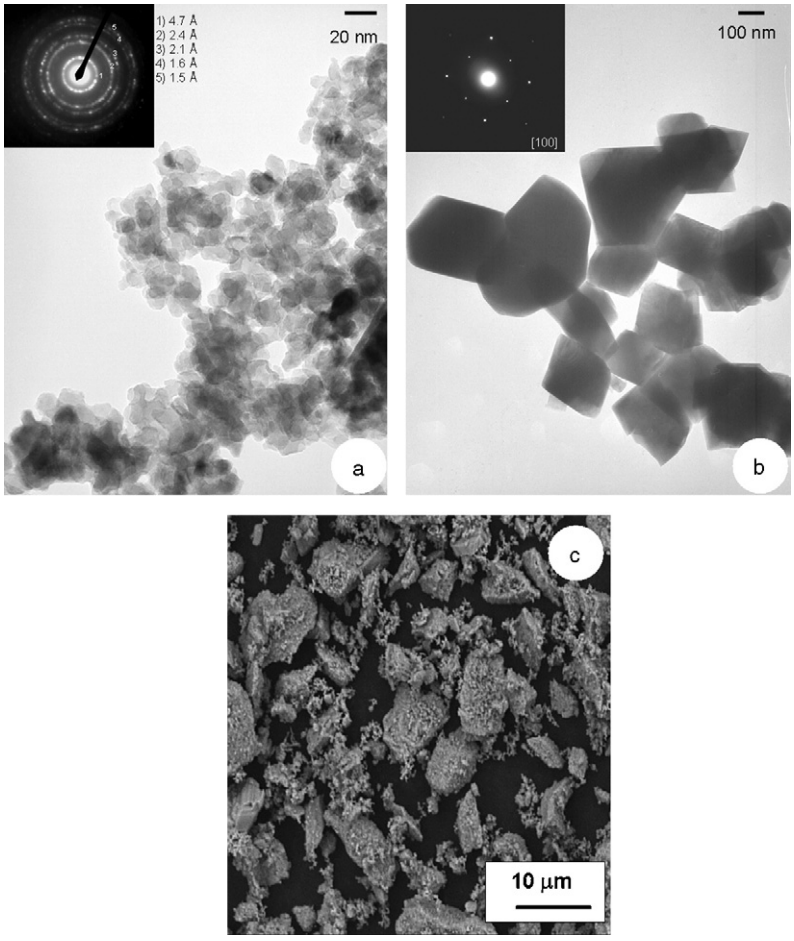

Fig. 2. (a) Typical TEM image of particles in the nano-$LiMn_2O_4$ spinel. SAED is shown in the inset with the diffraction rings exhibiting *d*-values corresponding to the cubic $Fm\bar{3}m$ $LiMn_2O_4$ spinel: (1) (1 0 0), (2) (3 1 1), (3) (4 0 0), (4) (5 1 1), (5) (4 0 0). (b) TEM image of the micro-$LiMn_2O_4$ spinel. (c) SEM image of the micro-$LiMn_2O_4$ spinel. SAED of the (1 0 0) plane is shown in the inset.

voltages, whose fingerprint can be clearly observed as a *plateau* at 4.8 V in the sample cycled at *C*/20, accounts for the difference in the coulombic efficiencies and capacity values, although the latter could also be ascribed to a more limited use of the active material when the charge–discharge rate increases.

Another effect of these side processes can be observed when several charge–discharge cycles are performed, as shown in Fig. 3d. While the initial discharge capacities are similar, a higher drop after 30 cycles (21% versus 10%) is observed when the rate chosen is *C*/20. This suggests that the electrode mixture underwent further degradation due to reactions with the electrolyte when a slow rate was used.

At this point, in order to assess the advantages of working with samples at the nanoscale, cycling at *C*/2 was carried out on $LiMn_2O_4$ prepared by the conventional solid state method (micro-$LiMn_2O_4$). The first cycle of this experiment is shown in Fig. 3c, and the results of cycling are also included in Fig. 3d. The specific capacity obtained upon charge is 118 mAh g^{-1}, similar to that of the nanometric sample, with 95% coulombic efficiency on discharge, which is only slightly lower than that of the $LiMn_2O_4$ prepared by the template method (nano-$LiMn_2O_4$). Thus, lithium diffusion in this material is already very good and working with a smaller particle size does not represent any noticeable improvement at these rates. Furthermore, when this micrometric sample was charged and discharged several times, a smaller capacity loss of 6% was obtained after 30 cycles. This behaviour of micro-$LiMn_2O_4$ reveals that harmful undesired reactions have a critical effect at this rate and that a lower surface area in contact with the electrolyte is probably more beneficial.

Nevertheless, these results also suggest that the decomposition reactions in the case of particles at the nanometric scale can be reduced by using higher rates of charge–discharge. In order to evaluate this hypothesis, the same type of experiment was performed at 2*C* for both samples, the results of which can be seen in Fig. 4. The first charge capacity yielded by the nanometric sample, 113 mAh g^{-1}, is significantly higher than that of the micrometric sample, 105 mAh g^{-1}. Additionally, the observed coulombic efficiencies, 97% for the nanometric and 92% for the micrometric sample, are also slightly improved when working with lower particle size and fast rates. Hence, in this case, the well known enhanced lithium diffusion in the small particles of the compound prepared by the template method has a significant effect.

Finally, the results of performing several cycles at 2*C* for both samples are shown in Fig. 4c. The tendency observed at

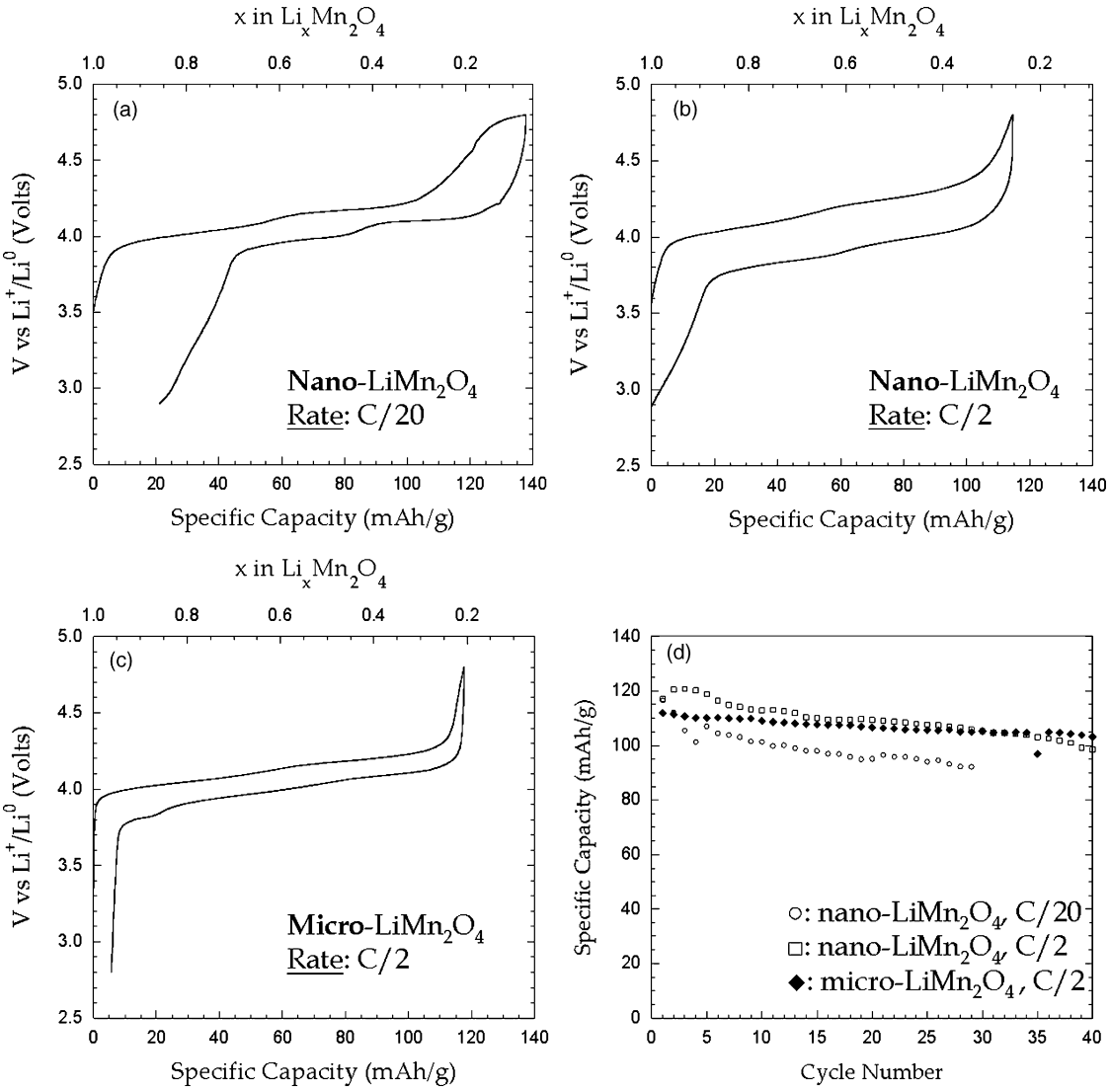

Fig. 3. Voltage-composition profile in the first cycle of an electrode containing: (a and b) nanometric $LiMn_2O_4$ cycled at a rate of C/20 and a *C*/2, respectively; (c) micrometric $LiMn_2O_4$ cycled at a *C*/2 rate; (d) comparison of the evolution of capacity upon cycling.

C/20 and *C*/2 is confirmed at 2*C* for nano-$LiMn_2O_4$, as only 2% of its capacity is lost after 30 cycles, much less than in the first two experiments. A similar phenomenon had been reported before by Caballero et al. [35] but no explanation was given. The main cause of the improved performance may again be related to a decrease in the extent of the irreversible side reactions with the electrolyte at high voltages, as indicated by the absence of the plateau at 4.8 V at *C*/2 and 2*C*. To support this hypothesis, the coulombic efficiencies at cycles 5, 10, 15 and 25 for each of the experiments performed with nano-$LiMn_2O_4$ are shown in Table 1. It can clearly be seen that, at low regimes such as *C*/20, the undesired processes catalyzed by the small particles that constitute this sample result in the consumption of a higher proportion of charge upon the oxidation of the electrode which is not recovered on reduction. As the maintenance of the battery at higher voltages is known to be detrimental for the integrity of the electrode due to undesired side reactions, fast charge rates, and, consequently, shorter times at these voltages would lead to a better cycling efficiency of the electrode material. However, the fact that this 4.8 V-*plateau* can be avoided if the charge is fast enough could also mean that the kinetics of the reactions with the electrolyte are slower than that of the diffusion of lithium in the small nanoparticles prepared by our template method, confirming that they can be minimized by increasing the current density. This is an interesting result, as it opens up new possibilities for nanostructured electrodes.

Furthermore, such an improvement would also result in a better performance of the nanometric sample compared to the micrometric sample at 2*C*. The loss of capacity when the micrometric sample is cycled (13%) is higher than when it is cycled at *C*/2, due to kinetic limitations on the lithium diffusion in the large particles that make up this sample. Although side processes may still occur to a larger extent in nano- than in micro-$LiMn_2O_4$, the enhanced lithium diffusion compensates for their occurrence and brings about an improved performance. Indeed, after 50 cycles, a difference of 20 mAh g^{-1} (100 mAh g^{-1}, for the nanometric, versus 80 mAh g^{-1}, for the micrometric) is observed between both samples. All these results lead to the conclusion that nano-

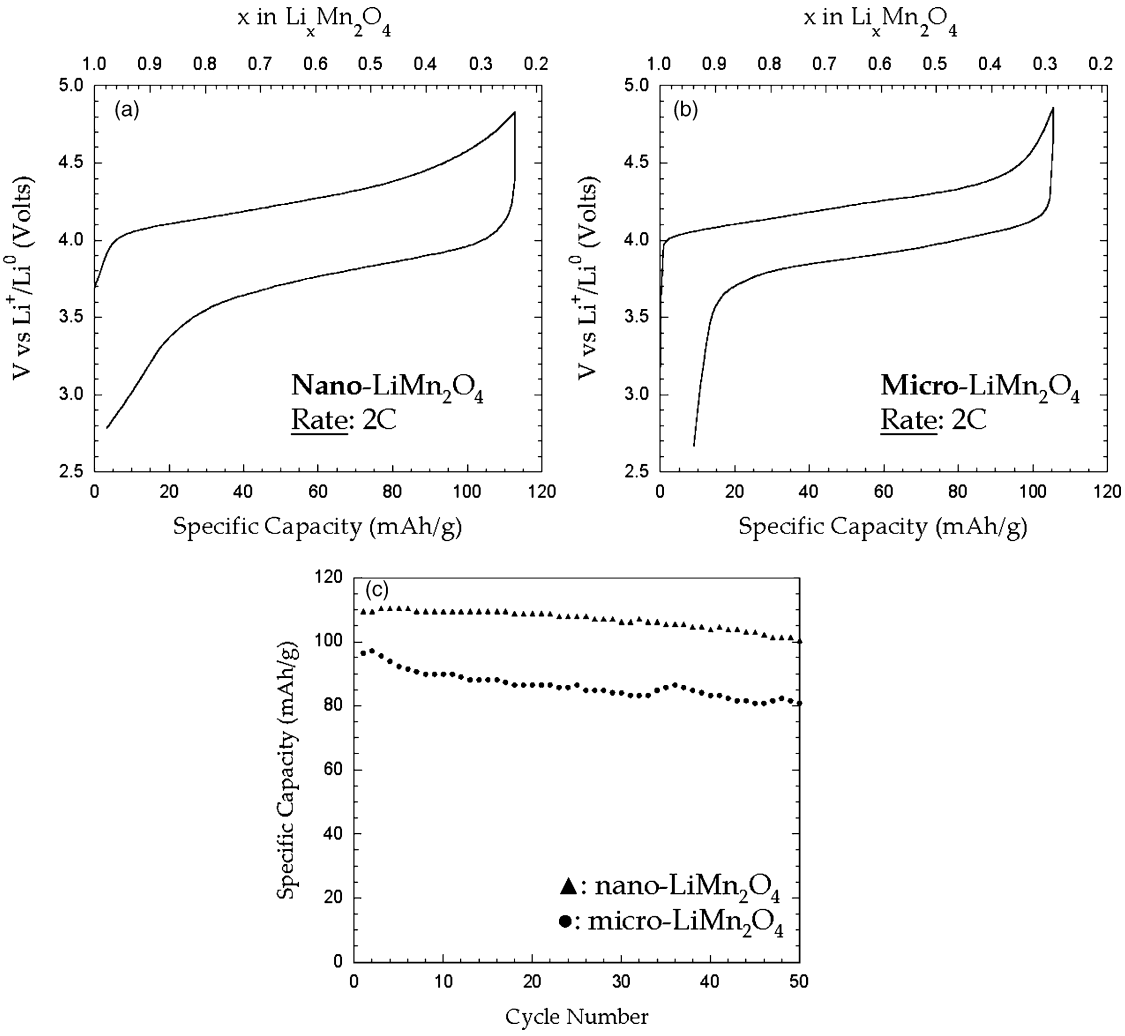

Fig. 4. Voltage-composition profile in the first cycle of an electrode containing: (a) nanometric $LiMn_2O_4$; (b) micrometric $LiMn_2O_4$, both cycled at a rate of 2*C*; (c) comparison of the evolution of capacity upon cycling.

sized $LiMn_2O_4$ synthesized by the novel template method shows much improved performances at fast rates of charge–discharge than when it is prepared by traditional solid state routes, making it a suitable subject for further research and optimization as a positive electrode in lithium batteries. In general terms, the results of this study agree with many recent studies in this and other compounds that explore the possibility of enhancing the electrochemical properties of both traditional and new electrode materials by reducing the particle size. High regimes could then be achieved, and the traditional drawbacks of lithium batteries, such as low power densities, could then be overcome.

Table 1
Coulombic efficiencies (%) at selected cycles observed when nano-$LiMn_2O_4$ prepared by the template method was charged/discharged at the rates indicated

Cycle #	*C*/20	*C*/2	2*C*
1	84.6	100	97.0
5	85.4	97.4	98.2
10	87.1	98.3	100
15	87.8	98.3	100
25	89.8	98.5	99.1

4. Conclusions

In summary, a novel synthetic route for obtaining nanosized $LiMn_2O_4$ spinel based on the template approach is reported. An inexpensive and readily available porous silica gel is used as hard template. The $LiMn_2O_4$ spinel obtained in this way is made up of single crystal nanoparticles with sizes between 8 and 20 nm. The electrochemical properties of this material in lithium cells were tested at different cycling rates up to 2*C*. It was found that its capacity retention improves with the increasing current density, most probably due to a reduction of the catalyzed side reactions with the electrolyte. Moreover, the electrochemical capacities obtained outperformed those of microsized $LiMn_2O_4$ at high rates (2*C*), capacity retention also being higher, with only 2% loss after 30 cycles. The results obtained open up new avenues for research. On the one hand, the same synthetic route could serve to enhance the properties of other materials. On the other hand, this study shows that detrimental processes enhanced by high specific surfaces can be minimized at fast rates in the case of $LiMn_2O_4$, making this compound more attractive as an eventual choice in

battery technologies where high rates are the main requirement.

Acknowledgements

Dr. Heiner Santner is thanked for his assistance in carrying out the electrochemical experiments. TVS thanks CSIC-ESF for the award of a postdoctoral I3P contract. The financial support for this research provided by the Spanish MCyT (MAT2005-00262) is gratefully acknowledged.

References

[1] T. Nagaura, K. Tozawa, Prog. Batteries Solar Cells 9 (1990) 209.
[2] J.M. Tarascon, M. Armand, Nature 414 (2001) 359.
[3] P. Poizot, S. Laruelle, S. Grugeon, L. Dupont, J.M. Tarascon, Nature 407 (2000) 496.
[4] M.M. Thackeray, P.J. Johnson, L.A. Depicciotto, P.G. Bruce, J.B. Goodenough, Mater. Res. Bull. 19 (1984) 179.
[5] M.M. Thackeray, A. Dekock, J. Solid State Chem. 74 (1988) 414.
[6] M. Yonemura, A. Yamada, H. Kobayashi, M. Tabuchi, T. Kamiyama, Y. Kawamoto, R. Kanno, J. Mater. Chem. 14 (2004) 1948.
[7] M.M. Thackeray, Prog. Solid State Chem. 25 (1997) 1.
[8] G. Amatucci, J.M. Tarascon, J. Electrochem. Soc. 149 (2002) K31.
[9] M.S. Whittingham, Chem. Rev. 104 (2004) 4271.
[10] K. Amine, J. Liu, S. Kang, I. Belharouak, Y. Hyung, D. Vissers, G. Henriksen, J. Power Sources 129 (2004) 14.
[11] D.H. Jang, S.M. Oh, J. Electrochem. Soc. 144 (1997) 3342.
[12] P. Reale, S. Panero, B. Scrosati, J. Electrochem. Soc. 152 (2005) A1949.
[13] A.S. Aricò, P. Bruce, B. Scrosati, J.M. Tarascon, W. van Schalkwijk, Nat. Mater. 4 (2005) 366.
[14] D. Larcher, C. Masquelier, D. Bonnin, Y. Chabre, V. Masson, J.B. Leriche, J.M. Tarascon, J. Electrochem. Soc. 150 (2003) A133.
[15] K. Du, H. Zhang, J. Alloy Compd. 352 (2003) 250.
[16] D. Kovacheva, H. Gadjov, K. Petrov, S. Mandal, M.G. Lazarraga, L. Pascual, J.M. Amarilla, R.M. Rojas, P. Herrero, J.M. Rojo, J. Mater. Chem. 12 (2002) 1184.
[17] K. Matsuda, I. Taniguchi, J. Power Sources 132 (2004) 156.
[18] S.H. Ye, J.Y. Lv, X.P. Gao, F. Wu, D.Y. Song, Electrochim. Acta 49 (2004) 1623.
[19] C.J. Curtis, J.X. Wang, D.L. Schulz, J. Electrochem. Soc. 151 (2004) A590.
[20] J.H. Choy, D.H. Kim, C.W. Kwon, S.J. Hwang, Y.I. Kim, J. Power Sources 77 (1999) 1.
[21] S. Nieto, S.B. Majumder, R.S. Katiyar, J. Power Sources 136 (2004) 88.
[22] C.W. Kwon, M. Quintin, S. Mornet, C. Barbieri, O. Devos, G. Campet, M.H. Delville, J. Electrochem. Soc. 151 (2004) A1445.
[23] Y. Zhang, H.C. Shin, J. Dong, M. Liu, Solid State Ionics 171 (2004) 25.
[24] H.M. Wu, J.P. Tu, X.T. Chen, Y. Li, X.B. Zhao, G.S. Cao, J. Electroanal. Chem. 586 (2006) 180.
[25] Z.P. Guo, J.H. Ahn, H.K. Liu, S.X. Dou, J. Nanosci. Nanotechnol. 4 (2004) 162.
[26] A.H. Lu, F. Schuth, C R Chimie 8 (2005) 609.
[27] F. Schüth, Angew. Chem. Int. Ed. 42 (2003) 3604.
[28] M. Schwickardi, T. Johann, W. Schmidt, F. Schüth, Chem. Mater. 14 (2002) 3913.
[29] A.B. Fuertes, J. Phys. Chem. Sol. 66 (2005) 741.
[30] B.Z. Tian, X.Y. Liu, H.F. Yang, S.H. Xie, C.Z. Yu, B. Tu, D.Y. Zhao, Adv. Mater. 15 (2003) 1370.
[31] T. Valdés-Solís, G. Marbán, A.B. Fuertes, Chem. Mater. 17 (2005) 1919.
[32] J.M. Tarascon, W.R. Mckinnon, F. Coowar, T.N. Bowmer, G. Amatucci, D. Guyomard, J. Electrochem. Soc. 141 (1994) 1421.
[33] B. Ammundsen, G.R. Burns, M.S. Islam, H. Kanoh, J. Roziere, J. Phys. Chem. B 103 (1999) 5175.
[34] C.M. Julien, M. Massot, Mater. Sci. Eng. B 100 (2003) 69.
[35] A. Caballero, M. Cruz, L. Hernan, M. Melero, J. Morales, E.R. Castellon, J. Power Sources 150 (2005) 192.